A comparison of human skin strain fields of the elbow joint for mechanical counter pressure space suit development

Edward W. Obropta
Massachusetts Institute of Technology
77 Massachusetts Ave. Cambridge, MA 02139
617-253-5487
eobropta@mit.edu

Dava J. Newman
Massachusetts Institute of Technology
77 Massachusetts Ave. Cambridge, MA 02139
617-258-8799
dnewman@mit.edu

Abstract—**A comparison of high-resolution human skin strain field data at the elbow joint measured using three-dimensional digital image correlation (3D-DIC) is presented. Developing skin-tight space suits requires detailed understanding of human skin deformation at joints in order to fit and create mechanical counter pressure without restricting human mobility. Previously, skin strain has been measured at 1 cm^2 resolution for one or two subjects to demonstrate the measurement technology. Now using 3D-DIC, skin strain is measured at 1 mm^2. Methodology to take these measurements and the data analysis is explained in detail. This paper goes beyond the measurement technology and presents data from four subjects and compares skin strain fields of the elbow joint, which gives insight into patterns and differences between varying anthropometrics and other factors that affect skin strain. These results are important to develop mechanical counter pressure space suits that are sized correctly for each astronaut and do not inhibit locomotion. These results are discussed in the context of realizing a mechanical counter pressure space suit designed for planetary exploration.**

TABLE OF CONTENTS

1. INTRODUCTION

In order to experience space first hand, we need space suits to protect us from the extreme environment. The current space suits are problematic for planetary exploration because they limit astronaut mobility and cause fatigue and exhaustion [1]. In the mid-1900s, Arthur Iberall researched ways to develop mobile pressurized space suits. He was inspired by the deformation and motion of human skin and developed the concept of the Lines of Non-extension (LoNEs), which he described as contours along the human body where the skin does not stretch [2]. Annis and Webb also developed approaches to make mobile space suits. They developed the Space Activity Suit, a mechanical counter pressure (MCP) space suit that used material elasticity to pressurize the body instead of gas pressure. They tested this concept in 1971, but

the gas pressurized suits were more technologically feasible at the time [3]. In 2001, the concept of a fully MCP space-suit reemerged at the Massachusetts Institute of Technology (MIT) as the Bio-Suit, which was inspired by Iberall, Annis, and Webb [4,5]. The concepts of MCP have also been applied to different components of space suits, such as gloves that have been tested by Tanaka *et al.* [6].

The energy required to arbitrarily deform a space suit can be expressed as:

$$\Delta W = \Delta W_p + \Delta W_b + \Delta W_s, \tag{1}$$

where the work required to change the gas pressure and volume of the suit is ΔW_p, the work to bend the suit's material is ΔW_b, and the work required to stretch the suit's material is ΔW_s [2]. Gas pressurized suits cause fatigue because they are difficult to move and bend primarily because of work done to change the pressure-volume, ΔW_p . Contrarily, MCP suits eliminate this term. This makes the mobility of MCP suits directly dependent on the mechanical deformation of the suit's material [7]. If the material is designed to deform similarly to the skin of the human body it is feasible that these factors can be minimized to make MCP suits have superior mobility. This is a challenging issue because the surface of the body undergoes a wide range of large, complex motions and deformations, which makes it difficult to model, engineer, and manufacture a MCP suit that maximizes mobility.

Research on skin deformation and physiology dates back to the mid-1800s with one of the earliest publications by Karl Langer [8]. Langer studied the skin of cadevers and created diagrams that shows the direction in which the skin deforms when punctured. The directions and lines are known as Langer Lines. Space suit and bio-medical research has progressed our understanding of skins deformation characteristics. The skin deformation at the knee joint was analyzed for the Bio-Suit [9–11] and for lower-limb prostheses [12]. Skin deformation at the ankle joint during flexion-extension and inversion-eversion was studied for development of active orthotics [13, 14]. This body of research has developed various techniques to quantify skin strain using laser-scanning and motion capture systems. Up until now the measurements have been limited to 1 cm^2, which limits the ability to compute LoNEs. It was difficult to analyze multiple subjects because of the large amount of manual data processing.

The overall goal of this research is to understand the human body's natural skin strain field in order to drive the design of a MCP space suit that maximizes mobility. By measuring the skin strain field, materials and textile patterns can be developed to engineer a second skin-like garment that deforms similarly to skin and does not restrict the mobility of the

Table 1. Subject Anthropometrics (cm)

Subject	A	B	C	D
Forearm length	26.5	29	24	24
Upperarm length	34	33	28.5	32
Bicep circumference (relaxed)	31	29	22.5	29
Bicep circumference (flexed)	34	32	24	30.4
Forearm circumference	27	25.5	19.5	26.5

Figure 1. **Speckle pattern applied to the skin (left). The base coat is a white Crayola Tempera paint applied with a brush and the top is a black Crayola Tempera paint applied with a speckle stamp. The 3D printed speckle stamp was made on a Makerbot Replicator 2X out of ABS plastic. (right)**

Figure 2. **Four cameras and one light were attached to a tripod in an arc configuration to view the elbow joint. The cameras were focused at the elbow joint, the area of interest (AOI). The rig was attached to the wall so that the elbow joint of each subject remained in the camera's AOI. The elbow joint angle is denoted as θ and could be fixed and measured by the rig using a protractor.**

astronaut. Using the skin strain field, the LoNEs described by Arthur Iberall can be quantitatively analyzed and used to engineer aspects of a MCP suit that utilize LoNEs. This research is also applicable to the bio-medical field. Skin deformation data can be used in tissue engineering to design synthetic skin for plastic surgery. It can be also used to design exoskeletons, prostheses, and orthotics that interface with skin to maximize comfort and mobility. The data can also be used to determine placement of body-worn sensors that have noise artifacts from skin deformation. The specific aim of the research in this paper was to develop a methodology to effectively measure skin strain and calculate LoNEs in an efficient way that can be scaled to analyze the LoNE map of the entire body and compare skin strain fields of multiple subjects.

The contribution of this work is the methodology to measure skin strain using 3D-DIC, a refined mathematical definition of LoNEs using streamlines, multiple calculation tools, and the first insight into how LoNEs vary between test subjects. Now, using three dimentional digital image correlation (3D-DIC) strain can be measured near 1 mm^2. Results are presented and discussed in the context of realizing a mechanical counter pressure space suit for planetary exploration.

2. METHODS

Experimental Design

Skin deformation and strain at the elbow joint of the human body was measured for four subjects (n=4, age: μ=22.3 years, σ=3.0 years) using three-dimensional digital image correlation. The subjects were male and female, had various anthropometrics, and varying skin tones. The anthropometrics are listed in Table 1. The forearm length was measured from the lateral epicondyle to the styloid process of ulna, the upperarm length was measured from the acromion to the lateral epicondyle, and the bicep and forearm circumference was measured at the largest circumference along the limb.

To perform 3D-DIC, a unique surface texture is required that is sufficiently random [15]. A speckle pattern was applied to the skin to create a unique texture. White Crayola Tempera was painted on with a brush. After the white paint dried, black Crayola Tempera paint was applied using a 3D printed speckle stamp. These paints were used because they are non-toxic and easily washable. An example of the applied texture on skin and the 3D printed stamp is shown in Figure 1.

Four cameras (Basler acA2500-14gm, GigE, monochromatic, 5 megapixel) were placed about the elbow joint in an arc configuration such that nearly 180° of the joint was viewable. The cameras were synchronized using hardware triggering. Figure 2 shows the camera and mechanical rig setup.

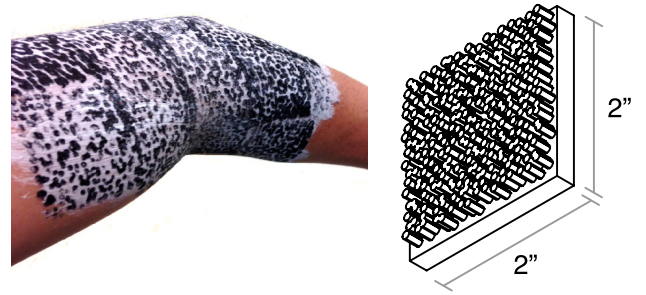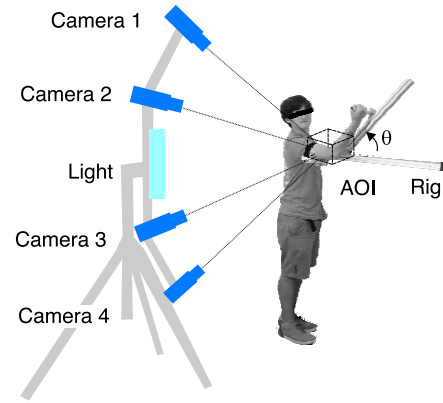Prior to data collection, the camera system was calibrated

using a black and white dot pattern of a known size, which was used to determine the optical properties of the cameras and the stereoscopic geometry. The cameras remained fixed throughout the entire data collection period so multiple calibrations were not necessary and all data would be collected in the same coordinate system. Each subject placed their right arm on a mechanical rig that allowed full range of elbow flexion and extension. The rig assured consistency of the arm positioning for all subjects. Each subject was positioned at increments of 15° joint angles using the mechanical rig starting at 0° elbow flexion to their maximum elbow flexion angle, which was typically 135°. All subjects were instructed to keep their palms facing upward throughout elbow flexion so that each subject's musculature would be similar.

Data Analysis

Digital image correlation calculates the full strain field of the surface of the object. Ultimately this strain field can be used to calculate the LoNEs as originally described and shown by Arthur Iberall [2]. This section describes the data analysis process after obtaining strain data through 3D-DIC to LoNE calculations in detail. Figure 3 shows an overview of the data analysis process.
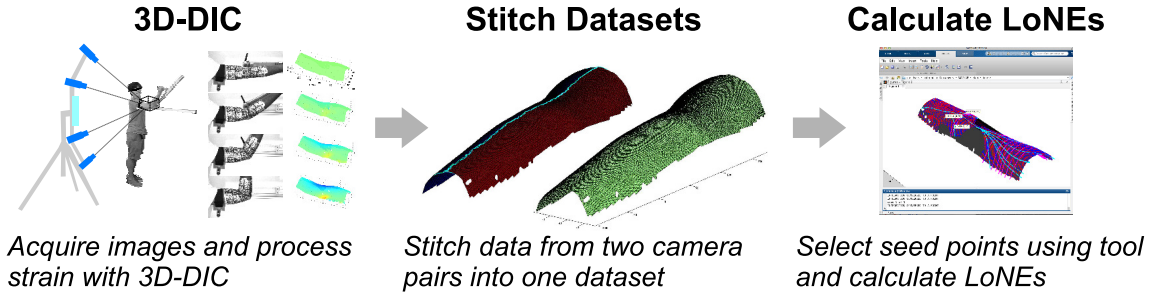
3D-DIC

Stitch Datasets

Calculate LoNEs

Acquire images and process strain with 3D-DIC

Stitch data from two camera pairs into one dataset

Select seed points using tool and calculate LoNEs

Figure 3. **Flow chart of data analysis from image acquisition to data visualization.**

The images were initially acquired using the MATLAB (Mathworks Inc., Natick, Massachusetts) image acquisition toolbox. The images were processed using VIC-3D, a commercial 3D-DIC software (Correlated Solutions Inc., Columbia, South Carolina). The commercial code calculates the displacement of pixel subsets in stereoscopic pairs of images. These displacements are used to calculate the strain of the surface. A subset size of 71 pixels was suggested by the software and used with a step size of 7 pixels. Green-Lagrange strain and Euler-Almansi strain was calculated with a Gaussian filter size of 15. In VIC-3D, this process can only be performed with stereoscopic camera pairs, therefore this process is repeated twice for a four camera system (Camera 1-2 and Camera 3-4). The data was exported to MATLAB to be further processed. Once the data is in MATLAB, the two datasets for each stereoscopic pair are converted from a curvilinear grid data type into a triangular mesh (vertices and triangular faces). The two triangular meshes are stitched together at their overlap using an algorithm inspired by Wuttke [16]. The four camera data can now be analyzed as one dataset. The strain field from VIC-3D is calculated using a local two dimensional coordinate system and the out-of-plane strain components, E_{13}, E_{23}, E_{33}, are assumed to be zero. The strain tensor,

$$\mathbf{E} = \left[\begin{array}{cc} E_{11} & E_{12} \\ E_{12} & E_{22} \end{array} \right] \qquad (2)$$

becomes 2D in the local coordinate system.

The principal strain directions are calculated by an eigenvector analysis of the local strain field at each data point where $\vec{v}$ are the eigenvectors and λ are the eigenvalues of the strain tensor:

$$\mathbf{E}\vec{v} = \lambda \vec{v} \qquad (3)$$

. The eigenvalues λ_1 and λ_2 are referred to as E_1 and E_2, respectively.

From the principal strain directions the directions of non-extension can be calculated by Equation 4 where ϕ is the angle from the principal strain direction. Note that directions of non-extension only exist if compression and tension are both present. Mathematically this is when E_1 and E_2 have opposite signs.

$$\phi = tan^{-1}\left(\sqrt{-\frac{E_1}{E_2}} \right) \qquad (4)$$

To conceptually understand this calculation we refer to the Finite Strain Ellipse and Mohr's Circle in Figure 4. Refer to
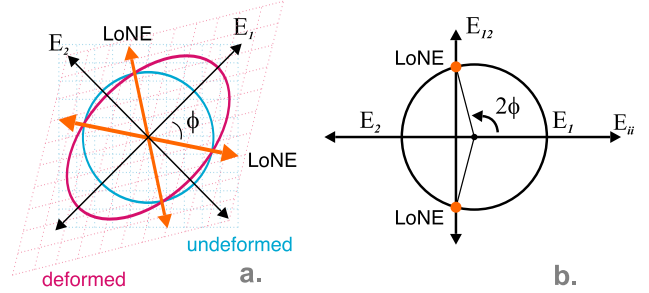

a.

b.

Figure 4. **The Finite Strain Ellipse (a) and Mohr's Circle (b). The ellipse shows how lines can develop called the Lines of Non-Extension (LoNE). There is no extensional strain along these lines, which is shown graphically in the ellipse, but also analytically in Mohr's circle. LoNEs only develop when the two principal strains have opposite signs, which means the material is undergoing tension in one direction and compression in an orthogonal direction.**

the Appendix for a derivation of Equation 4 and a discussion of the relation between Finite Strain Ellipse and Mohr's Circle techniques for progressive deformations.

The directions of principal strain and non-extension are now described as 2D vectors, however they need to be transformed into 3D. The commercial code computes the strain field with respect to a local 2D coordinate system on the surface of the object. The local coordinate system has the basis vectors $\mathbf{e_i'}$ and the global coordinate system has the basis vectors $\mathbf{e_i}$. The local coordinate system is defined with $\mathbf{e_3'}$ aligned along the surface normal vector, $\mathbf{e_1'}$ has no component along $\mathbf{e_2}$ and is orthogonal to the surface normal, and $\mathbf{e_2'}$ is the remaining orthogonal direction, $\mathbf{e_3'} \times \mathbf{e_1'}$. Using Equation 5 the vector fields can be rotated into the global reference frame. $\mathbf{X'}$ is local 2D vector field to be rotated, $\mathbf{X}$ is transformed the global 3D vector field, and $(\mathbf{e_j} \cdot \mathbf{e_i'})$ is the direction cosines. This is then expressed as $\mathbf{R}$, the rotation matrix.

$$\mathbf{X_i} = (\mathbf{e_j} \cdot \mathbf{e_i'})\mathbf{X_j'}$$
$$cos\theta_{ji} = \mathbf{e_j} \cdot \mathbf{e_i'} \qquad (5)$$
$$\mathbf{X} = \mathbf{R}\mathbf{X'}$$

At this point there are four vector fields in the global frame, the first and second principal strain directions and the first and second lines of non-extension directions. The last step is to visualize these vector fields.

LoNE Visualization

A LoNE is a contour that remains tangential to the non-extension direction. Once the non-extension directions have been calculated in 3D we can visualize the LoNEs. Previously, the lines were calculated discreetly by finding neighboring elements that have similar vector directions and connecting them. The results of this process were affected by the mesh sizing and mesh connectivity [11, 13, 17]. To correct this problem, a continuous approach was taken by treating the LoNE directions as a vector field and integrating the vector field as streamlines tangential to the surface. Because the vector field is not technically a velocity field the time step used in the integration is not technically a time step, but can be considered a spatial parameter. This calculation requires interpolation of the vector field at each time step to determine the vector field at the integration point. First the vector field must be linearly interpolated. The k-nearest neighbors, S, (in this case k=9), were transformed to the local tangential coordinate system using Equation 6.

$$\mathbf{S}' = \mathbf{R}^{-1}\mathbf{S}$$
$$\mathbf{S}' = \mathbf{S}' - \langle \mathbf{S}' \rangle \tag{6}$$

Once the k-nearest neighbors are in the local coordinate frame they are used to bilinearly interpolate the components of the vector field, $\mathbf{u}$. This process is completed using a least-squares approach, which is shown by Equation 7, where $\bar{u}(x,y)$ is the interpolated vector field.

$$\mathbf{u}(x,y) = a + bS'_x + cS'_y + dS'_xS'_y$$
$$\mathbf{u}(x,y) = \begin{bmatrix} 1 & S'_{x1} & S'_{y1} & S'_{x1}S'_{y1} \\ \vdots & \vdots & \vdots & \vdots \\ 1 & S'_{xk} & S'_{yk} & S'_{xk}S'_{yk} \end{bmatrix} = \mathbf{a}$$
$$\mathbf{u}(x,y) = \mathbf{A}\mathbf{a} \tag{7}$$
$$\bar{\mathbf{a}} = (\mathbf{A}^{\mathbf{T}}\mathbf{A})^{-1}\mathbf{A}^{\mathbf{T}}\mathbf{u}(x,y)$$
$$\bar{\mathbf{u}}(x,y) = \bar{a} + \bar{b}x + \bar{c}y + \bar{d}xy$$

This interpolated vector field is used to calculate streamlines. In the streamline calculation the current position plus the velocity at that point multiplied by a time step is the new position. One additional complexity is that our vector field lies along a surface and is neither 2D or completely 3D. In order to solve this problem the integration must be carried out using a local 2D coordinate system and continually transforming the coordinates to 3D. This process is carried out in Equation 8.

$$\mathbf{X}'_{\mathbf{i}} = \mathbf{R}^{-1}\mathbf{X}_{\mathbf{i}}$$
$$\mathbf{X}'_{\mathbf{i+1}} = \mathbf{X}'_{\mathbf{i}} + \bar{\mathbf{u}}(\mathbf{X}'_{\mathbf{i}})dt \tag{8}$$
$$\mathbf{X}_{\mathbf{i+1}} = \mathbf{R}\mathbf{X}'_{\mathbf{i+1}}$$

One down side of streamline vector field visualization is that the calculation requires selecting seed points. There is a large body of work on selecting seed points to produce equally space streamlines [18]. To avoid this complexity a seed point
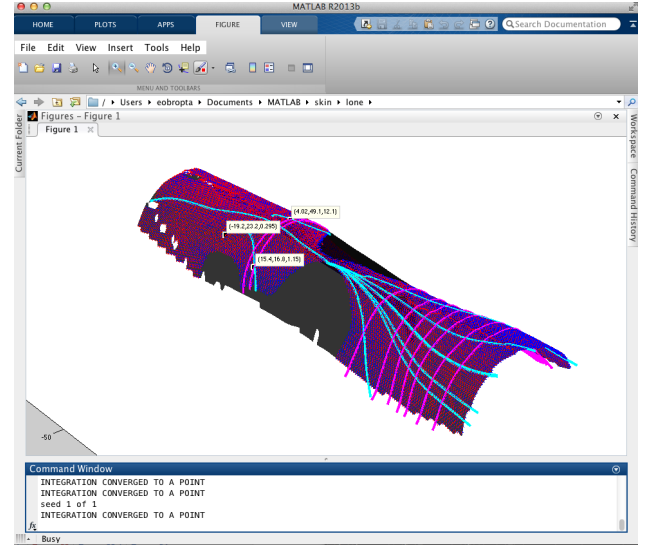

Figure 5. **Interactive LoNE tool for seed point selection that augments the MATLAB data cursor.**

selecting tool was developed in MATLAB, which is shown in Figure 5. The tool augments the ability of the MATLAB data cursor in order to select and then subsequently visualize each LoNE.
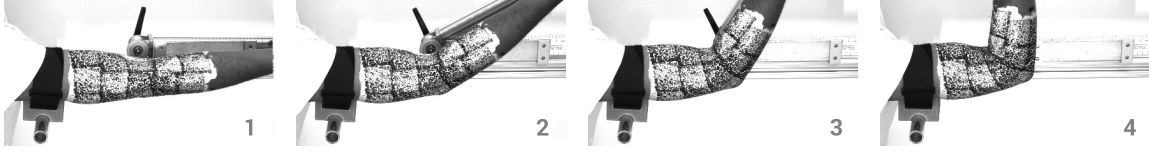
3. RESULTS

The results are divided into two sections. The first section, *Subject A*, looks in-depth at the strain data from test subject A. All of the steps in the data analysis process are shown for test subject A starting at the strain magnitude and ending at the determination of LoNEs. The second section, *Subjects A-D*, shows only the LoNE maps for test subjects A through D. Note that all strain data is Green-Lagrangian strain and shown in the undeformed reference frame.
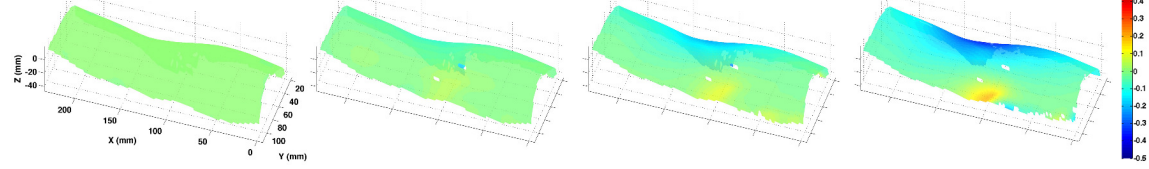
Subject A

The data for one subject is shown in Figure 6. The elbow joint angles are 0, 30, 60, 90° increasing from left to right. The data analysis is shown incrementally from top to bottom. The first row shows the the raw images taken from one of the four synchronous cameras. The second row shows the magnitude of the second principal Green-Lagrange strain. The surface is always represented in the undeformed configuration. The data shows that near the tip of the elbow the Green strain reaches 0.3. The third row shows the principal directions of the strain. The red is always used for the first principal strain direction and the blue is for the second principal strain directions. These directions are orthogonal. The fourth row shows the LoNEs that were calculated for the direction of non-extension. There are two LoNE directions which are shown by the red and blue lines. The light blue areas of the surface denote regions that do not have LoNE directions, which is when E_1 and E_2 have the same sign.

Principal directions can also be visualized as lines using the same methodology that was applied to the directions of non-extension. These lines are referred to as the lines of principal strain. Figure 7 shows the LoNEs and the lines of principal strain projected onto the deformed configuration at 90° elbow flexion. The lines were calculated using the strain field at 90° elbow flexion. The projection was calculated by applying the
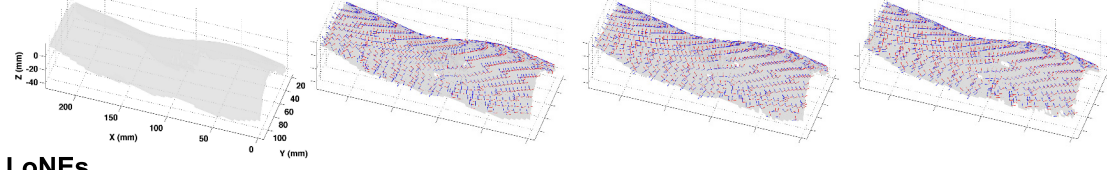
4

Raw Images

Principal Strain Magnitude

Principal Strain Directions
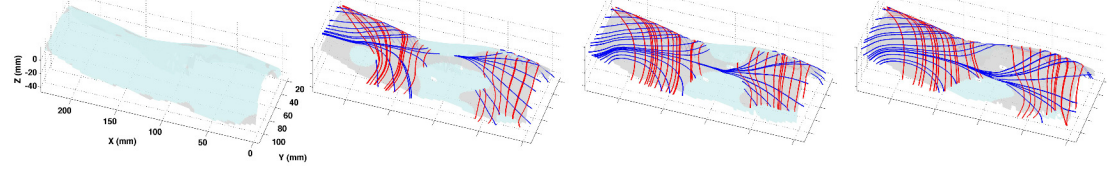

LoNEs

Figure 6. **Strain results of one subject. The elbow joint angle increases from left to right in 30° increments from 0° to 90°. The data processing is shown incrementally from top to bottom. Row 1: the raw images from one out of the four cameras, row 2: the magnitude of the second principal Green strain, row 3: the principal strain directions as vectors (red corresponds to the first principal strain and blue corresponds to the second principal strain), and row 4: the first and second LoNEs shown respectively in red and blue.**
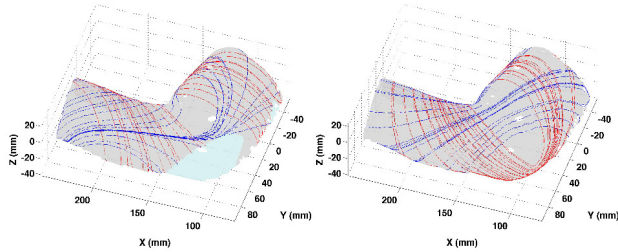

Figure 7. **LoNEs (left) and lines of principal strain (right) are shown in the deformed configuration at 90° elbow flexion. The red and blue represent the first and second directions of non-extension for the LoNEs and first and second lines of principal strain.**

local displacement vector to each point that makes up a line.

LoNEs are assumed to remain at a consistent length throughout deformation. To check this assumption, the LoNEs calculated at 90° elbow flexion were projected to all other deformations. The Euclidean arc length was calculated for each LoNE at each deformation. Figure 8 shows the average change of the length of each LoNE with standard deviation error bars. For comparison the same process was carried out for the lines of principal strain. The sample size was 54 LoNEs and 46 lines of principal strain, where 8 lines of principal strain were not considered because they could not be successfully projected.

Table 2. Range of Principal Strain

Subject	A	B	C	D
E_i (min)	-0.41	-0.43	-0.34	-0.44
E_i (max)	.46	.36	.49	.60

Subjects A-D

The strain field for subjects A through D was measured. The range of principal strain is reported in Table 3, which shows the large range of strain experienced by human skin.

The LoNEs for four subjects are shown in Figure 9. The LoNEs were calculated when the elbow joint was at 90° for each subject using similar locations for the seed points. The LoNEs are shown in the undeformed configuration. The data for is not scaled between subjects so the results presented are in their original coordinate system with a translation applied to visualize each subject separately.

4. DISCUSSION AND CONCLUSION

The strain field was measured near 1 mm^2 resolution using 3D-DIC and the LoNEs were calculated as continuous streamlines using an interactive seed point selection tool. Figure 10 shows the progression on skin strain research in the context of mechanical counter pressure space suits. Starting from Karl Langer in 1861, skin strain can now be measured at high resolution and directional information such as LoNEs
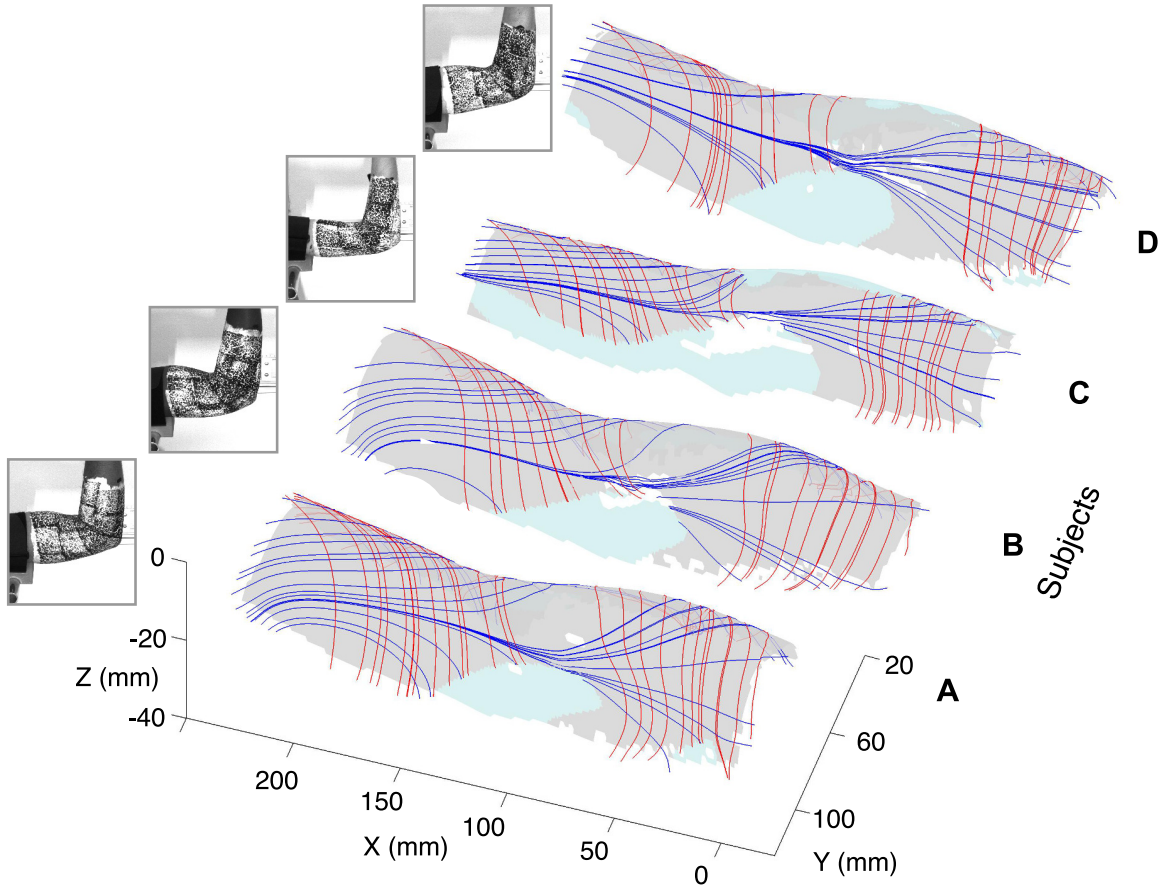
Figure 9. LoNEs for multiple subjects are shown for when the elbow is at $90°$. The results are shown on the undeformed configuration. The seed points used for each subject were in relatively similar locations. There are two LoNE directions which are shown by the red and blue lines. The light blue areas of the surface denote regions that do not have LoNE directions.
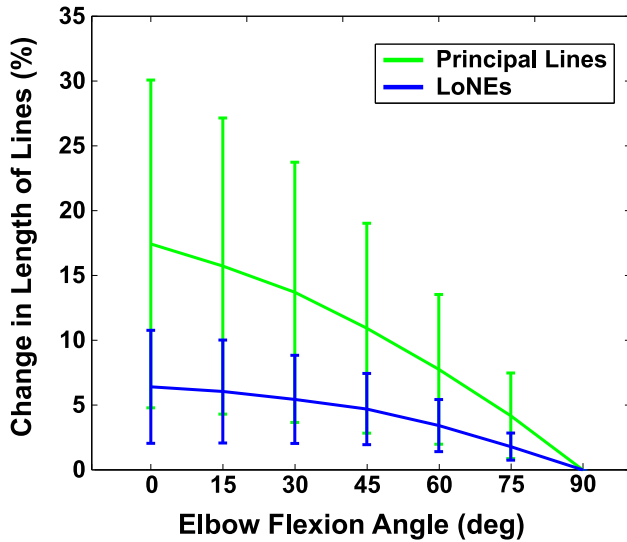

Figure 8. Average change in the length of LoNEs and lines of principal strain shown throughout the deformation. The error bars represent the standard deviation of the mean. LoNES: n=54, Lines of principal strain: n=46.
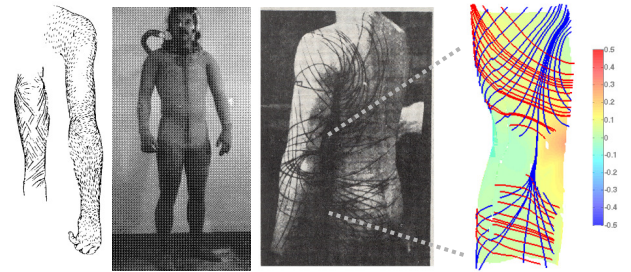

Figure 10. The progression of research in the context of mechanical counter pressure space suits. From left to right: Langer Lines for the right arm [8], the Space Activity Suit demonstrating the feasibility of MCP space suits [3], the Lines of Non-extension as determined by Iberall in pursuit of making a mobile pressure suit [2], and the present work with the first principal strain measured at 1 mm^2 with LoNEs overlaid.

can be quantified and visualized.

LoNEs can be computed and visualized for each state of deformation. Different deformations could result in different LoNE maps. Iberall stated, "Experimental study of the intrinsically limited motion at each joint verifies that this system of lines of non-extension will be essentially the same

6

for all deformations [2]." This phenomenon is now shown quantitatively in Figure 8 for the elbow. On average, LoNEs remain within 6% of their original length when projected back to 0° elbow flexion whereas lines along the principal directions changed 17%. Indeed LoNEs change length when examined throughout the deformation, but these lines undergo a minimum amount of extension when compared to other lines that could be drawn on the surface, such as lines through the principal directions.

The LoNE map was successfully mapped for multiple subjects. Despite, varying subject anthropometrics, the LoNE maps look similar between subjects. In Figure 9 the blue set of LoNEs seems to consistently converge along the brachioradialis muscle. This suggests that is may be possible to develop a model to predict the LoNE map of an individual, which would significantly improve the ability to rapidly develop custom garments. This is important because even though there are a small number of astronauts now, if humans are to colonize another planetary body, many custom suits will need to be manufactured. The LoNE map is being used to create textile patterning for the Bio-Suit at MIT. The data is also being used minimize the strain in wearable technology systems that are placed on the body. This research can also be applied to the field of tissue engineering and to design and develop soft exoskeletons, soft prostheses, and soft orthotics that interface with skin.

There are various limitations with this research. One limitation is the inability to draw widespread conclusions from a small sample size of four subjects. Now that a method has been developed to measure skin deformation more subjects will be tested. Another limitation is that a method for analyzing error in the data and LoNE maps still needs to be developed. A significant amount of computational power is required for 3D-DIC, which limits it's ability to become a real-time system. It is also difficult to analyze large sections of the body at the same time because of the body's sophisticated geometry. Already four synchronous cameras are being used, but the full elbow joint cannot be mapped at once.

In the future, the LoNE map will be analyzed for more sections of the body. This field has studied the elbow, knee, and ankle (flexion-extension, inversion-eversion). The next joint to study will probably be the shoulder. Unlike the elbow and knee, the shoulder has various degrees of freedom that will have to be taken into account in the experimental design, similarly to the ankle. The data from the elbow can be extended up to the shoulder. With an entire arm mapped, the data will be used to design and develop a MCP arm sleeve that can be compared against gas-pressurized space suit arms. In addition to measuring skin deformation at other joints, a method for quantitatively comparing LoNE maps between subjects will be developed. An attempt will be made to develop a model of the LoNE map that is a function of human subject variables such as anthropometrics. Once a method is developed it will be tested on elbow data collected here with the addition of more subjects. This is critical to design MCP suits that fit without measuring each subject. The LoNE geometry and model will be used to develop the next version of the MIT Bio-Suit.

APPENDICES

The direction of non-extension, ϕ, that is used to calculate the LoNEs in Equation 4 is derived. In Iberall's description

of LoNEs he states, '"The twofold extended mapping of such diameters are principal shear lines, here to be called 'lines of non-extension.' Along these two lines we may lay strands of "infinite modulus" (i.e., there is no stretch) [2]." This technique is also found in geology. Ramsay *et al.* quantifies the lines of non-extension directions [19], but its derivation is not complete. The derivation shown here will relate the finite strain ellipse and Mohr's circle. The derivation shows that the LoNE directions do not occur at the maximum shear directions as specified by Iberall. The maximum shear direction is always 45° from the principal strain, which is shown visually by Mohr's circle. Figure 11 shows the finite strain ellipse and Mohr's circle where λ_1 and λ_2 are the principal stretches and λ is stretch at a point on the ellipse. The direction of non-extension is denoted as ϕ. In the diagram $\lambda = 1$, which means it has no extension.

Using the equation of an ellipse the stretch, λ, can be calculated at any point along the ellipse

$$
\frac{x}{\lambda_1}cos^2\phi + \frac{y}{\lambda_2}sin^2\phi = 1
$$
$$
\lambda = \lambda_1 cos^2\phi + \lambda_2 sin^2\phi
$$

(9)

To find the direction of non-extension set $\lambda = 1$ and solve for ϕ using the trigonometric identity $cos^2(\phi) + sin^2(\phi) = 1$.

$$
1 = \lambda_1 cos^2\phi + \lambda_2 sin^2\phi
$$
$$
cos^2\phi + sin^2\phi = 1
$$
$$
sin^2\phi = \frac{1 - \lambda_1}{\lambda_1 - \lambda_2}
$$
$$
cos^2\phi = \frac{1 - \lambda_2}{\lambda_1 - \lambda_2}
$$
$$
tan^2\phi = \frac{sin^2\phi}{cos^2\phi}
$$
$$
tan\phi = \sqrt{\frac{-(\lambda_1 - 1)}{\lambda_2 - 1}}
$$

(10)

The principal stretches can be written as strain using the relations $\lambda_1 = e_1 + 1$ and $\lambda_2 = e_2 + 1$, which results in Equation 4.

$$
tan\phi = \sqrt{\frac{-e_1}{e_2}}
$$

(11)

Note that the strains are the infinitesimal strains, which is the assumption that finite strain ellipse is small enough to have a homogeneous deformation. Because the data is measured near 1 mm^2 using 3D-DIC the assumption is made that the strain is locally homogeneous.

Equation 4 can also be derived using Mohr's circle. Referring to Figure 11, R is the radius of Mohr's circle and w is the distance to the center of Mohr's circle.
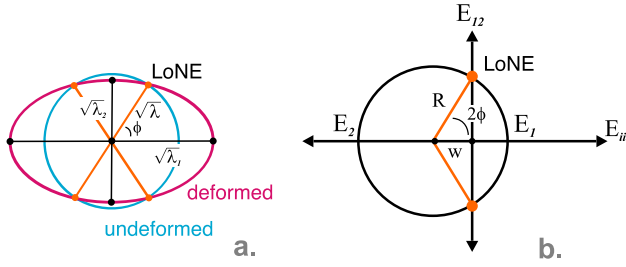
Figure 11. **The finite strain ellipse (left) and Mohr's circle (right).**

$$cos2\phi = w/R$$
$$R = \frac{e_1 - e_2}{2}$$
$$w = e_2 + R \qquad (12)$$
$$cos2\phi = e_2/R - 1$$
$$cos2\phi = \frac{e_1 + e_2}{e_1 - e_2}$$

Using the trigonometric identities $cos2\phi = 2cos^2\phi - 1$ and $cos2\phi = -2sin^2\phi + 1$ we find

$$sin^2\phi = -\frac{1}{2}\left(\frac{e_1 + e_2}{e_1 - e_2} - 1\right)$$
$$cos^2\phi = \frac{1}{2}\left(\frac{e_1 + e_2}{e_1 - e_2} + 1\right) \qquad (13)$$

then using $tan^2\phi = sin^2\phi/cos^2\phi$ we arrive back to Equation 4

$$tan\phi = \sqrt{\frac{-e_1}{e_2}} \qquad (14)$$

REFERENCES

[1] L. D. Kozloski, *U.S. space gear: outfitting the astronaut*. Washington: Smithsonian Institution Press, 1994.

[2] S. Iberall, "Experimental design of a mobile pressure suit," *Journal of Basic Engineering*, vol. 92, no. 2, pp. 251–364, 1970.

[3] J. F. Annis and P. Webb, "Development of a space activity suit," NASA, Report, 1971.

[4] B. Pitts, J. Brensinger, C. andSaleh, C. Carr, P. Schmidt, and D. Newman, "Astronaut bio-suit for exploration class missions," Massachusetts Institute of Technology, Report, 2001.

[5] D. J. Newman, M. Canina, and G. L. Trotti, "Revolutionary design for astronaut exploration - beyone the bio-suit system," pp. 975–986, February 2007.

[6] K. Tanaka, P. Danaher, P. Webb, and A. R. Hargens, "Mobility of the elastic counterpressure space suit glove," *Aviation Space Environmental Medicine*, vol. 10, no. 0095-6562 (Print), pp. 890–3, 2009.

[7] C. E. Carr and D. J. Newman, "Space suit bioenergetics: Framework and analysis of unsuited and suited activity," *Aviation Space and Environmental Medicine*, vol. 78, no. 11, pp. 1013 – 1022, 2007.

[8] K. Langer, "On the anatomy and physiology of the skin," *British Journal of Plastic Surgery*, vol. 17, no. 31, pp. 93–106, 1861.

[9] K. Bethke, D. J. Newman, and R. Radovitzky, "Creating a skin strain field map with application to advanced locomotion spacesuit design," 2005.

[10] N. Wolfrum, N. D.J., and K. Bethke, "An automatic procedure to map the skin strain field with application to advanced locomotion space suit design," Cleveland, OH, July 2006.

[11] A. M. Wessendorf and D. J. Newman, "Dynamic understanding of human-skin movement and strain-field analysis," *Ieee Transactions on Biomedical Engineering*, vol. 59, no. 12, pp. 3432–3438, 2012, wessendorf, Ashley M. Newman, Dava J.

[12] A. T. Marecki, "Skin strain analysis software for the study of human skin deformation," Thesis, Massachusetts Institute of Technology, 2012.

[13] A. R. Domingues, J. Martins, M. SIlva, and D. Newman, "Analysis of the human ankle impedance for the design of active soft orthosis," August 2013.

[14] S. P. Marreiros, A. R. Domingues, J. Martins, M. T. Silva, and D. J. Newman, "Computational calculation and representation of the lines of non-extension of the ankle-foot complex," June 2013.

[15] H. W. Schreier, J.-J. Orteu, and M. A. Sutton, *Image Correlation for Shape, Motion and Deformation Measurements : Basic Concepts, Theory and Applications*. New York, N.Y.: Springer, 2009, accession Number: 277000. Publication Type: eBook. Language: English.

[16] S. Wuttke, D. Perpeet, and W. Middelmann, "Quality preserving fusion of 3d triangle meshes," pp. 1476–1481, 9-12 July 2012.

[17] A. R. Domingues, S. P. Marreiros, J. M. Martins, M. T. Silva, and D. J. Newman, "Skin strain field analysis of the human ankle joint," February 2010 2010.

[18] T. McLoughlin, R. S. Laramee, R. Peikert, F. H. Post, and M. Chen, "Over two decades of integration-based, geometric flow visualization," *Computer Graphics Forum*, vol. 29, no. 6, pp. 1807–1829, 2010.

[19] J. G. Ramsay, M. I. Huber, and R. J. Lisle, *The techniques of modern structural geology*. London; New York: Academic Press, 1983.

BIOGRAPHY

Edward Obropta *received the Bachelor of Science degree in aerospace engineering in 2013, and is currently pursuing a Masters of Science degree in aeronautics and astronautics, from the Massachusetts Institute of Technology (MIT). His research interests include bioastronautics, space suit design, solid mechanics, active materials, bio-medical devices, and sports technology.*

Dava Newman *received the Bachelor of Science degree in aerospace engineering from the University of Notre Dame in 1986, the Masters of Science degree in aeronautics and astronatics in 1989, and the Masters of Science degree in technology and policy in 1989, and the Ph.D. degree from the Massachusetts Institute of Technology (MIT) in aerospace biomedical engineering in 1992. She is currently a Professor in the Department of Aeronautics and Astronautics and Engineering Systems at MIT and affiliate faculty in the Harvard-MIT Health Sciences and Technology Program. She leads research efforts in extravehicular activity (EVA) including advanced space suit design, musculoskeletal modeling, biomechanics and energetics, human-robotic co-operation, and biomedical devices. Her exoskeleton innovations are now being applied to 'soft suits' to study and enhance locomotion on Earth for children with Cerebral Palsy in addition to astronauts.*